In-situ observation to improve the analysis of the scratch damage of coated polymeric surfaces

Vincent Le Houerou, Leandro Jacomine, Christian Gauthier

Chapter 2

In-Situ Observation to Improve the Analysis of the Scratch Damage of Coated Polymeric Surfaces

Vincent Le Houérou, Leandro Jacomine and Christian Gauthier

Université de Strasbourg, CNRS
Institut Charles Sadron UPR 22
67 000 Strasbourg, France
v.lehouerou@unistra.fr

1. Introduction

Coatings are nowadays widely used to modify the properties of a substrate surface for various engineering purposes: electronic, optical, packaging, biomedical and decorative applications. Moreover, recent advances in coating technologies make possible the deposition of advanced thin films that were unavailable 10 years ago. The impact of these new deposition techniques is a promising variety of applications that emerge in an equally wide variety of technical domains. Although the coating solution has been successfully used for some time now, in order to obtain a specific surface function it needs also to ensure durability upon tribological demands. Some coatings (i.e. the anti-scratching coatings) have even as main function the protection of the substrates they are deposited on. Actually, the surface of substrates can elicit brittle behavior when submitted to scratching or wear, and this could constitute an important time-limiting factor. Then, a common way to enhance the mechanical and tribological performances upon contact consists in coating the substrate with an elastic thin film, which increases the elastic component in the elastic–plastic behavior of the assembly. However, one of the limitations of this method is the risk of cracking and chipping of the film. The origin of the success of the coating technique is still of research interest, and further works are still required to explain fully the benefits of the coating solution and predict the cracking risks. Indeed, the mechanical

responses of these coatings depend on the characteristics of coating, substrate and interface.

A sliding contact undergone by this kind of coated material can involve different deformation processes: (i) delamination (blister formation) and fracture (which may include chipping) of the coating and (ii) viscoelastic–viscoplastic deformation and fracture of the substrate. The difficulties in understanding deformation and damage in complex film/substrate systems lie in the following issues:

- Since the mechanical properties of polymeric materials are time and temperature dependent, one cannot determine a single value of the critical normal load of damage occurrence in the film.
- The adhesion of the coating, which governs the interfacial behavior, has not been very successfully determined yet.
- The contribution of the substrate to the deformation within thin polymer films remains largely to be studied.
- The geometric scales are of prime importance, since, for example, the thickness of the film relative to the contact area and/or the roughness of the scratching tip (which requires an exact knowledge of the tip shape) is critical for the mechanical behavior of the system [1].

Some clues and answers to these difficulties may be drawn from the literature, and these approaches will first be reported here for three different situations:

- Delamination of the coating: Thouless *et al.* [2] considered a circular blister in a thin film. A mode dependence of the blister propagation was found in experiments: mode II predominated over mode I as the interfacial crack propagated, so that the interface toughness increased as the blister grew. Hutchinson and Suo [3] examined the propagation of a straight-sided blister (i.e. only in one direction) like those leading, for example, to telephone-cord buckles [4]. More recently, Faou *et al.* [5] contributed further in the description and explanation of such damages. In a scratching process, Kriese *et al.* [6] described the establishment of a large delamination ahead of the indenter.
- Fracture of the coating: With or without prior delamination, fracture of the coating has been reported to involve various processes. Bull [7] and Bull *et al.* [8] found that, under some conditions, wedge cracks can form some distance in front of the indenter due to the large displacement of the coating caused by compressive stresses ahead of the indenter. Malzbender *et al.* [9] described a fracture of the coating in the form of two radial cracks [10, 11], as was also reported with delamination by Kriese *et al.* [6] and by

Venkataraman *et al.* [12] in a Pt thin film/NiO substrate system. Lastly, Bull [7] described the interfacial failure which results from the pile-up occurring in front of the moving indenter before the film buckles. Demirci *et al.* [1] observed that cracking of the coating may appear within the contact area, rather than at the rear edge, while the ratio of the contact radius to the radius of the grooving tip proved to be a relevant parameter to predict the damage and does not depend on the scratching velocity or temperature.

- Viscoelastic–viscoplastic deformation of the substrate: Gauthier *et al.* [13] have previously shown that the substrate deformation can be studied through the shape of the contact area between the indenter and the material. The rear contact is due to the elastic recovery of the polymer and depends on the plastic contribution to the elastic–plastic strain in a characteristic spherical volume of matter under the contact area. Ideally, a non-existent rear contact area leads to a perfectly plastic contact, while identical rear and front contact areas lead to a fully elastic contact. Intermediate cases give rise to elastic–plastic contacts.

In this context, the present chapter contributes to a better understanding of damages induced by scratching thanks to the *in-situ* observation. The three situations evoked previously will be described and discussed. Then, this chapter provides insight into the scratching behavior of two film/substrate systems with regard to experimental conditions (temperature and scratching speed). The geometric dimensions involved in the contacts were controlled in order to ensure viscoelastic/viscoplastic behaviors of the material assemblies and to examine the delamination and brittle failure of a coating. The single-asperity scratching device that was used allows *in-situ* observation of the scratch so that different fracture modes of the coating and/or the interface were pointed out in this chapter. The experimental observations are discussed in terms of the adhesion, the substrate contribution, the appearance of interfacial cracking and the delamination growth.

As mentioned previously, a crucial concern in the material response is the adhesion between the coating and the underlying substrate. Actually, the durability of coatings is intimately related to the adhesion that demands a precise understanding and measurement [8, 14]. The adhesion is characterized by the energy associated with an interfacial fracture between the film and the substrate. Of interest is how to measure this property of the assembly. Most of the methods for evaluating the adhesion of thin films to substrates [3, 8, 14–17] are semi-quantitative tests: they are not directly related to material mechanisms of adhesion and do not reproduce damage undergone by the coated surface during its real lifetime. The scratch test is

widely used to evaluate the scratch resistance of coatings. It is commonly accepted as being a convenient simplification for tribological and contact mechanical problems since it simply consists in dragging a well-defined tip on the sample surface while the applied normal load is controlled (constant, continuous or stepwise). The scratch test appears to be a good candidate to assess quantitatively the adhesion of coated systems [9, 18].

Depending on the test conditions, it will be reported further that it is possible to achieve a steady-state blistering propagation without cracking within the film, favorable to an energetic analysis as reported elsewhere [18, 19]. Indeed, the energy spent in the delamination process can be determined by following the delaminated area during the blistering process with regard to the scratching distance [18, 19]. Then, an energy balance approach will be applied to a photo-curing coating deposited on a mineral glass substrate. In order to cope with the difficulty in estimating the energy dissipated in plastic flow, different tests were conducted with various indenters: spheres with different radii and roughness. The global energy balance model coupled with this multi-indenter approach permits the determination of the adhesion of the system in the case of experimental stable blistering propagation. This chapter also aims to investigate the reliability of this energetic approach with regard to probe characteristics in the adhesion determination context.

2. Experimental Procedure

The scratch tester employed as well as the samples used to validate this method are described in this part. With regard to the samples, two kinds of systems have been studied: (a) hard layer coated over a compliant substrate, as for instance layers to reduce friction or groove formation during scratch tests under polymer glasses and (b) compliant layer deposited onto a hard substrate, such as for functional painting to protect surfaces against chemical or environmental aggressions. In these two systems, plasticity will influence differently: in the first, elastic strain will propagate through the layer and at the interface and then may generate plastic strain in substrate, whereas in the second plasticity will occur exclusively into the layer.

2.1. *Samples*

(a) Hard layer coated over a compliant substrate: A-type sample

The material was provided by a manufacturer of ophthalmology glasses and consisted of an amorphous polycarbonate with a nanocomposite coating (obtained by the dip-coating technique) composed of a thermoset matrix filled to about 20% of its volume with nanosized silica particles (about

10 nm in diameter). The samples received were circular in shape with a diameter of 80 mm, a total thickness of about 2 mm and a thin film thickness of 3.5 μm. They are fully transparent. The Young's modulus of the thin film were given by the manufacturer as 5.5 GPa. As it was to be used as a model material, the adherence of the system was not optimized during manufacture by omitting the cleaning process of the substrate before coating. Hence, the interfacial strength was expected to be weak. The mechanical properties of the polycarbonate substrate were determined by Dynamic Mechanical Analysis (DMA) using a standard tensile/compression machine (Instron). The compression samples are cylinders of diameter 5 mm and height 12.5 mm. The Young's modulus and Poisson ratio were measured as a function of temperature for three different frequencies: 0.05 Hz, 0.5 Hz and 5 Hz.

(b) Compliant layer deposited onto a hard substrate: B-type sample

Cationic photo-cured hybrid nanocomposites with covalent bonds between organic and inorganic networks were prepared by a concomitant UV curing process. This process based on concomitant sol-gel reaction and photopolymerization were prepared as described elsewhere [20]. Besides the usual advantages of cationic polymerization (insensitivity to oxygen inhibition, good adhesion and post-polymerization), this single step process appeared particularly interesting since crosslinking of both inorganic and organic parts of the liquid resin occurs simultaneously and rapidly under UV radiation at ambient temperature to generate a three-dimensional hybrid network.

The coatings were synthesized by adding organosilanes (bearing epoxy and trialkoxysilyl functional groups) to a cationic resin: EPALLOY 5000. Homogeneous formulation was prepared by mixing EPALLOY 5000 with 20 wt% of GPTMS and other additives [20]. Before UV irradiation, the hybrid photo-curable mixtures were applied onto mineral glass substrates by means of a bar coater. The resulting materials are fully transparent. For all experiments, an effective coating thickness of 15 μm was achieved. The adherence of the system was not optimized during fabrication and hence the interfacial strength was expected to be weak.

2.2. *The scratch test apparatus*

The scratch test apparatus has been fully described elsewhere [21] and is called the "microvisio-scratch" device (Fig. 1). It consists of a commercial servomechanism which provides the scratching action by moving the sample relative to the tip. Sample and tip are enclosed in a temperature-controlled

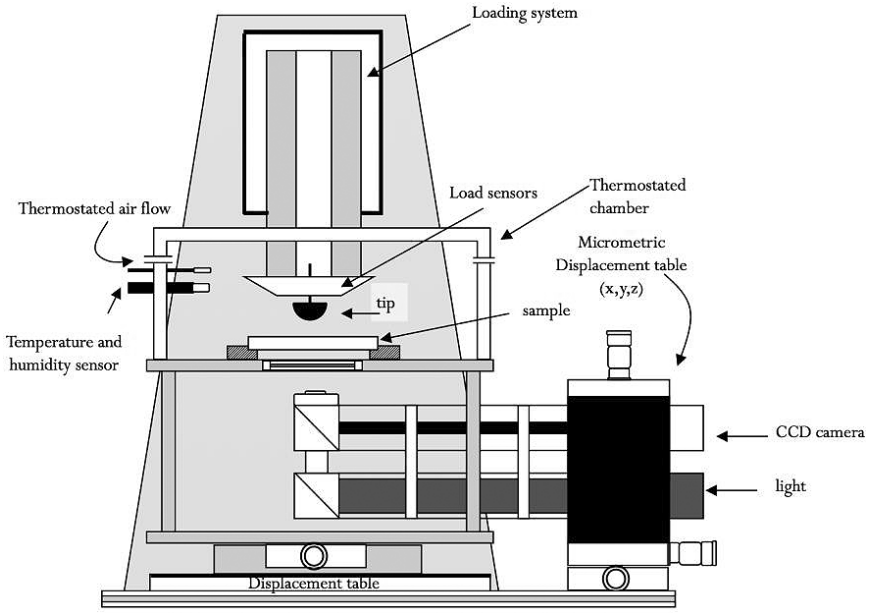

Fig. 1. Experimental setup used in this study, allowing for *in-situ* visualization if the sample is transparent.

transparent box allowing temperature dependence studies in the range −70–+120°C. The scratching velocity V_{tip} in the range 1–10^4 μm/s and the normal load F_n are also imposed, and all the test parameters, i.e. F_n, F_t (tangential load), V_{tip} and T (temperature), are continuously monitored and recorded during experiments. As a consequence, the apparent friction coefficient can be determined all along the test. The normal load applied to the tip is constant during each scratching step and can be adjusted stepwise from 0.05 to 25 N by compression of a flexible spring. It is possible to set as many steps as required to explore the desired strain range in a single experiment. A built-in microscope allows *in-situ* observation of the indenter/sample contact in the case of transparent samples. Additional details on the setup can be found in Ref. 22. Using this *in-situ* contact visualization, the damage processes were investigated for sliding contacts between the coated materials and a spherical indenter. Scratch tests have been performed at least three times for each test condition in order to ensure representativeness of measurements.

The first part of the results in this chapter deals with the rigid layer deposited onto the elastic–plastic polymer. The scratch tests were carried out with an indenter having a spherical radius R of 116 μm. The radius and the roughness were measured by profilometry ($R_t = 0.6\,\mu$m). One may note

that the ratio of the total roughness to the thickness of the film ensures no direct damage of the interface due to the tip roughness [1].

It appears that gentle cleaning of the sample with alcohol and drying before testing do not significantly affect the contact mechanical properties of the material. Caution must however be taken not to clean the samples too strongly since otherwise the film can partially delaminate. The indenter was also cleaned with alcohol and dried before experiments. A preliminary test was then performed to run in the surface of the tip with the polymer in order to obtain reproducible measurements according to Gauthier *et al.* [22] and in order to identify the normal load value needed to initiate the blistering process of the coating (value used as constant load to perform the second test). The tests were carried out for the following different temperatures: $-20°$C; $0°$C; $25°$C; $50°$C; $70°$C; $90°$C. The scratching speed was kept constant for each test and in the range: 3; 10; 30; 60; 100; 300 μm/s.

In the second part, which concerns the compliant coating deposited onto a mineral glass, the scratching speed was kept constant for all the tests at 10 μm/s. This scratch speed was chosen to prevent a perceptible time response of the material to loading during the tests: thus, the specimen could be considered as purely elastoplastic in the study.

Then, the damage processes were investigated for sliding contact between the coating and a set of spherical glass indenters. The latter have radii, R, of 250, 500 or 1,000 μm and varying roughness. Actually, this study needed different size of indenters made from optical lenses (R_a as received $\sim$0.005 μm), and for each size different roughness was necessary. To achieve this, one indenter of each size was sand blasted in a way that roughness of 1.4 μm was obtained (see Fig. 2) and measured on a white light confocal profilometer. Finally, the set of indenters was composed of six spheres: two roughness for each of the three sphere sizes. The indenters were ultrasonically cleaned in ethanol and dried with nitrogen flow before experiments. One may note that the ratio of the total roughness to the thickness of the film ensures no direct damage of the interface due to the tip roughness [1]. All the samples were taken from the same elaboration batch and no inconsistency of the films was pointed out.

3. Analysis of Damage of Coatings

3.1. *Mechanisms of the scratching damage*

An overview of the morphologies of delamination and cracking processes occurring during the scratching of a coated material was established through the example of the A-type sample [23]. This description is given for

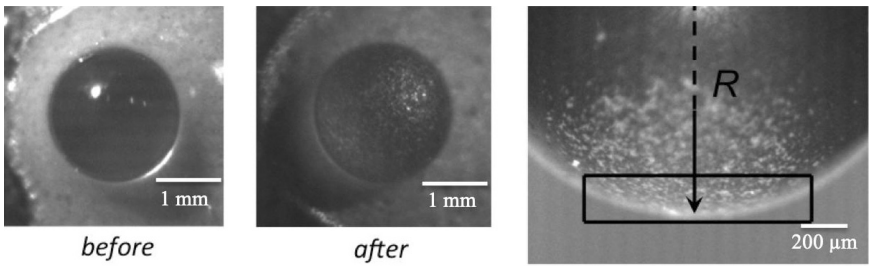

Fig. 2. Optical pictures of a $1,000\,\mu$m radius spherical tip. From left to right: as received (smoothed indenter); after sand blasting; the black rectangle shows the considered zone for the profilometry exploration.

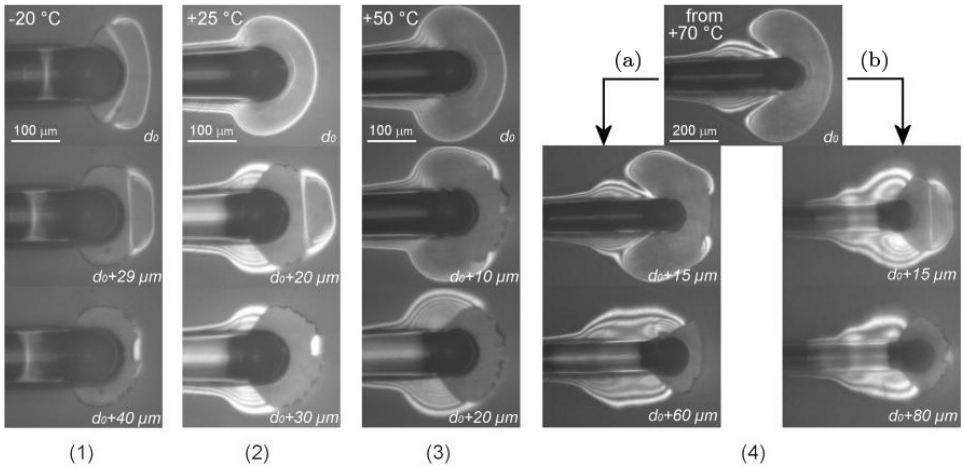

Fig. 3. Blistering and cracking sequences during scratching depending on the temperature.

the chosen experimental conditions. Four different sets of mechanisms of delamination and/or fracture of the thin film were identified, while the critical normal load ranged from 1.2 to 0.6 N with increasing temperature. Representative images of these mechanisms are shown in Fig. 3.

This overview may be described as follows:

(1) At -20°C: Two radial cracks occur at the rear side of the indenter/surface contact and propagate ahead in the thin film in both lateral directions. Finally, these cracks delineate a circular shape ahead of the indenter so that chipping occurs. This corresponds to the damage mechanisms evoked in the introduction and described by Malzbender [9]. One may note that chipping corresponds to material removal (only coating) due to cracking within the film; the substrate is not affected by cracking.

(2) At +25°C: A large delaminated circular surface or "blister" appears ahead of the indenter and on the outside edges of the remaining scratch track. As the indenter moves, two radial cracks occur and propagate similarly as in the previous case, leading to chipping as they unite to delineate the chip. A delaminated surface remains visible at the rear side of the indenter.

(3) At +50°C: A similar circular blister appears ahead of the indenter and the cracking sequence then starts right at the front of the blister through a buckling process. Chipping occurs when the cracks generated by the buckling have propagated back to the indenter from both sides of the scratch. As in the previous case, a delaminated surface remains visible at the rear side of the indenter.

(4) At +70°C and above: At the very beginning of the delamination/ cracking process, a circular blister grows in the same manner as in (2) and (3) but instead of cracking, it surprisingly continues to grow. After the indenter has advanced a few micrometers, the rear part of the blister separates from the scratching track on both sides. This peculiar-shaped blister grows at the same speed as the movement of the indenter relative to the surface, with the two lateral parts becoming larger and moving away from the scratch track. The phenomenon can last over several hundreds of micrometers and the blister can sometimes become too large to be observed on a single screen. On account of its characteristic shape, this kind of blister has been called a "crescent blister". A chronological sequence of the crescent blister growth is proposed in Fig. 4.

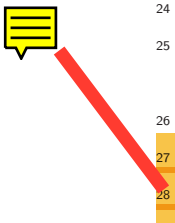

It highlights the fact that as the indenter passes, the thin film is plated back on the surface of the sample. The plated-back surface is indicated by the dashed lines in Fig. 4 (only represented on one side of the scratch). The crescent blister propagation ends when cracking suddenly occurs as reported in Fig. 3. Two modes of damage are observed and may be assimilated to the cracking processes of (2) and (3): (a) radial cracks appear at the rear side of the indenter/surface contact and propagate ahead in the thin film or (b) cracking occurs through buckling at the front of the crescent blister. The two modes lead to similar damage patterns with chipping ahead of the indenter and a large delaminated surface behind.

The appearance of this crescent blister at temperatures above +70°C is particularly interesting because the damage propagates stably over several hundreds of micrometers and enlarges significantly. At −20°C only mechanism (1) and above +70°C only mechanism (4) exist. Between +25°C

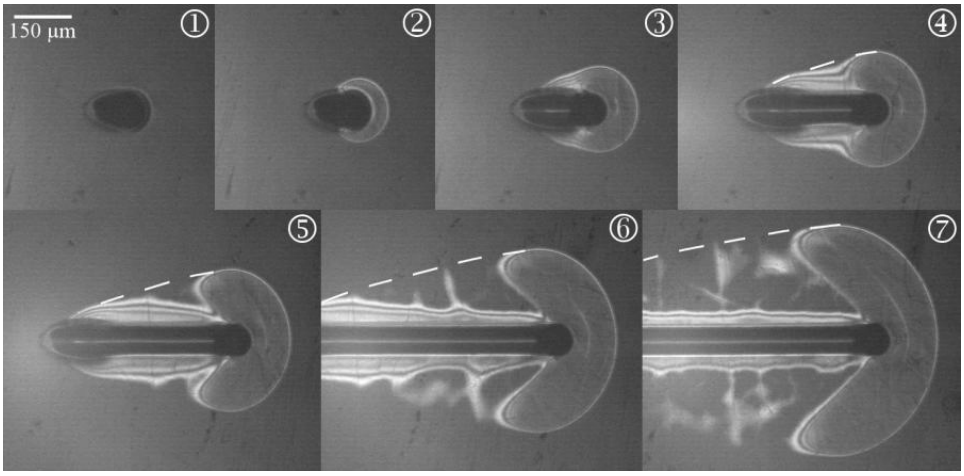

Fig. 4. Chronological sequence of the crescent blister growth during scratching of the material with 10 m/s scratching speed and a temperature of 90°C. The indexes (1)–(7) chronologically number the shots. The dashed lines indicate the part of the thin film which has been plated back onto the substrate.

and +70°C, mechanisms (2) and (3) may randomly occur, each of it with its own probability depending on temperature. Moreover, in the light of the numerous tests performed (at least 15 tests for each temperature condition), it seems reasonable to assume the previously described evolution with temperature.

One may note that the coating remain elastic during the scratching experiments since it does not exhibit plasticity contrary to the substrate.

3.2. *Dependence of the delaminated area on the temperature and scratching velocity*

The video sequences of the thin film damage recorded during scratching experiments enabled an image analysis of the created delaminated area. Thus, for each temperature and scratching speed, the video sequence images were analyzed and the blister and total delaminated areas were deduced. One of the difficulties was to identify the boundary between the blister and the contact area and the boundaries of the delaminated area. A semi-automatic procedure was used and gave reproducible results with a standard deviation of less than 4% between two area measurements on the same video sequence.

Figure 5(a) summarizes the results. In this figure, the total delaminated area (blister + "stuck back" area) is represented as a dashed line and the blister area as a solid line. The dashed and solid curves correspond to the scratching speed of 30 μm/s at each test temperature. The full range of

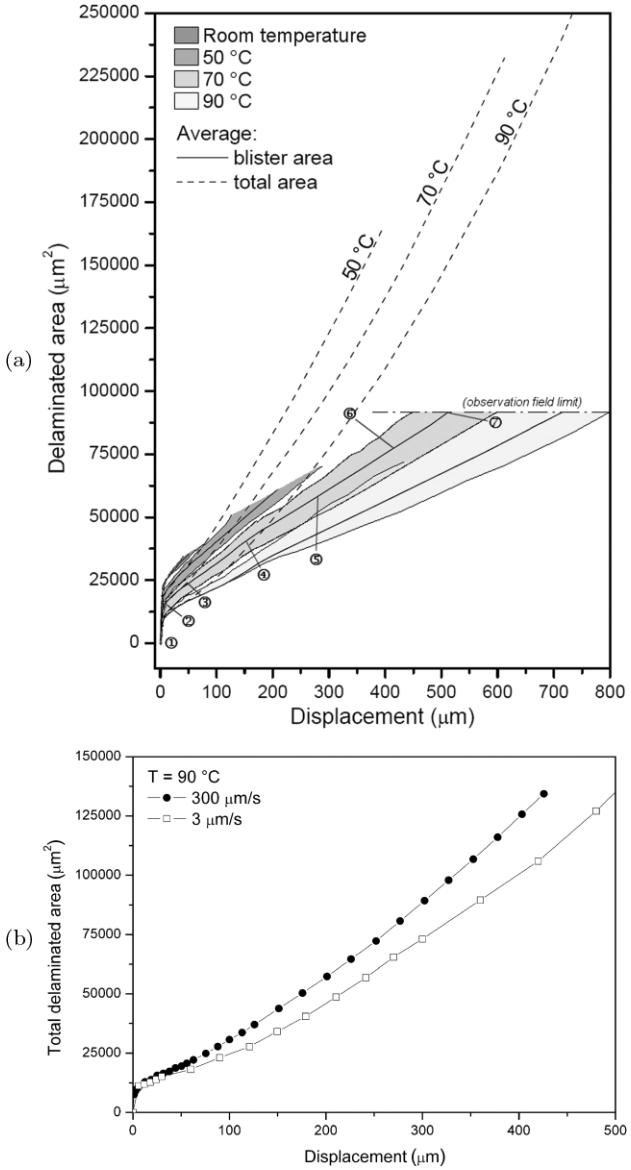

Fig. 5. (a) Delaminated area as a function of the scratching displacement for different temperatures and scratching speeds (deduced from the video sequences of scratching). (b) Time dependency of the total delaminated area as a function of the sliding displacement.

speed (3–300 μm/s) is reported as four curve groups represented by grey shades with respect to the four reported temperatures. The observation field limit corresponds to the maximum size of the pictures for the currently used magnification, which for some experiments, especially at high temperature,

did not allow further measurement of the delaminated area, since the blister ran over the screen borders while continuing to grow without fracturing. At room temperature and +50°C, failure of the film always occurred before the blister reached the maximum size of the screen.

After the initiation process, the total delaminated areas (dashed lines) seem to follow a second order polynomial function of the scratching distance, which is consistent with the shape of the delamination (approximately part of a circle of radius equal to the scratching distance). The increase in the blister area follows an evolution that is similar under all test conditions. The blistering starts with the initiation process at a high delamination rate over about the first 10 micrometers of scratching and subsequently the blister area increases with a constant slope that reflects a relatively stable propagation of the interfacial crack. One may note that the lower the temperature, the greater the rate of increase (characterized by the slope of the curve). Moreover, Fig. 5(a) shows four groups of curves related to the blister growth depending on the temperature: all the curves obtained for scratching speeds of 3–300 μm/s at a given temperature are included in the corresponding curve group. The results are consistent with the common time and temperature dependence of polymer properties, which states that a 20°C variation in temperature corresponds approximately to a variation of one to two decades in strain rate. Figure 5(b) emphasizes this fact by presenting the total delaminated area as a function of the displacement of the indenter for one temperature and two sliding speeds. It is encouraging to find a time and temperature dependency even if some difficulties persist to precisely distinguish the boundary between the blister and the contact area.

Figure 6 depicts the growth rate of the blister in the linear domain as a function of the true friction coefficient during scratching, at different test temperatures. The true/local friction coefficient was derived from the apparent friction coefficient, defined as the ratio of the tangential to the normal load (F_t/F_n) measured during scratching, using the procedure of Lafaye *et al.* [24] whereby the real-time geometry of the contact area must be experimentally measured and taken into account in the calculations. Since the precise real-time geometry of the contact area was not available during the blistering or cracking process, the measurements were made just before the occurrence of these phenomena and the friction coefficient was assumed to remain constant during the subsequent damage. Figure 6 shows that the growth rate of the blister increases as the temperature decreases, in accordance with the increase in the true/local friction with decreasing temperature. In fact, the blister growth rate and the true friction coefficient are intimately linked because the friction largely governs the blister growth.

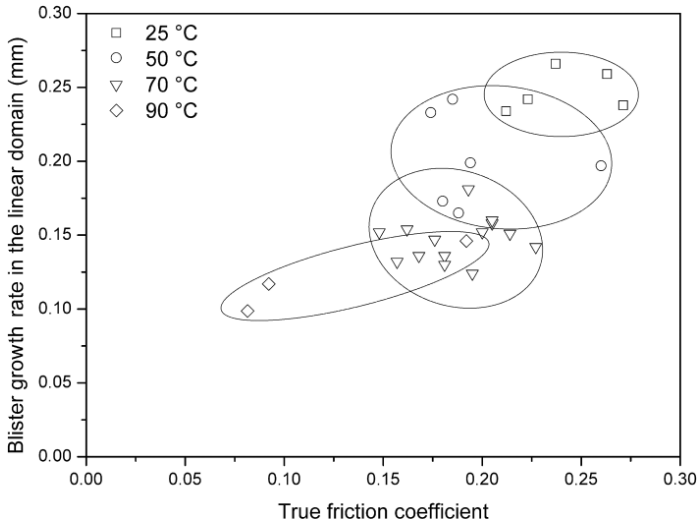

Fig. 6. Growth rate of the blister in the linear domain as a function of the true friction coefficient during scratching at various test temperatures. Surrounding circles with respect to the different temperatures have been added to the graph for reading convenience.

Since at the same time, the contact pressure during scratching increases as the temperature decreases [21], it may be worthy of note that the growth rate of the blister increases if the interfacial shear stress rises.

3.3. *Blistering mechanism*

Thus, under certain conditions of temperature and scratching speed, delamination can occur at a thin film/substrate interface. The toughness of the interface between the coating and substrate, the possible viscous character of the coating and substrate, the yielding of the substrate and the true friction between the moving indenter and the surface are the mechanical parameters controlling the blister. As no mechanical model describes up to now correctly the initiation and propagation of this kind of damage, the present analysis concerns mainly geometric lengths.

As is well known, an elastic deflection appears when an indenter penetrates a material and this deflection of the substrate seems to contribute greatly to the mechanism of delamination. An *in-situ* laser interferometric technique during the scratch can provide insight into this elastic deflection of the substrate as shown in Fig. 7(a). The concentric interference lines in the immediate vicinity of the indenter illustrate this elastic deflection since fringes arise from the laser reflections between the bottom of the sample and the upper surface of the substrate. The laser beam was 0.635 μm in wavelength and about four concentric interferometric fringes can be counted,

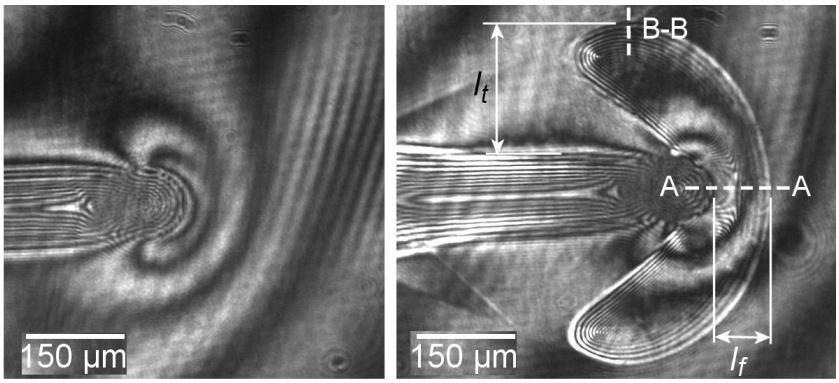

(a) (b)

Fig. 7. Laser interferometric images of a scratching indenter on the coated substrate (70°C). (a) Elastic deflection in front of the indenter. (b) Crescent blister showing the definitions of the front and transversal lengths (l_f and l_t) and the cross-sections A–A and B–B.

so as the elastic deflection was $1.3 \pm 0.3\,\mu$m since the inter-fringe equals to the half-wavelength of the laser. The residual track left behind the indenter shows a predominantly plastic scratch (no viscoelastic recovery behind the indenter [13]). No information can be easily derived from the interference patterns shown in the residual track: fringes are a complex compound of laser reflections.

As proven by Gauthier *et al.* [13], the elastic deflection of an elastic–fully plastic scratch can be estimated by classical laws of elastic contact in indentation. Hence, it is reasonable to consider in first approximation the deflection obtained when pressing a flat punch on the material, with the radius of the punch equal to the contact radius between the spherical indenter and the sample [25]. This expression is given by Sneddon [26]:

$$h_e = \frac{(1-\nu^2)}{2Ea} F_n, \tag{1}$$

where h_e is the elastic deflection depth, F_n is the normal load, E and $\nu$are the elastic parameters of the material and a is the contact radius. As the coating is very thin relative to the contact width, the elastic properties of the thin film do not significantly influence the substrate response and we may consider that this analytical expression approximates the deflection of the substrate during scratching with a spherical tip. At +70°C, corresponding to the example reported in Fig. 7, the Young's modulus and Poisson ratio of the polycarbonate were estimated to 2.15 GPa and 0.4, respectively, by DMTA technique (these values are the average results of the experiments

performed at different frequencies), the contact radius a was found to be $52\,\mu$m for a normal load F_n of 0.55 N and the calculated deflection is about $2.1\,\mu$m. The latter value is of the same order of magnitude compared to the measured value by interferometry and the difference comes from the fact that the experimental scratch is not a fully plastic scratch.

Once the deflection of the substrate has been introduced and estimated, the mechanism of the initiation of delamination can be explained with regard to the bulk behavior of the material. As illustrated in Fig. 8, during scratching of a perfectly plastic material with a spherical indenter, a frontal plastic push pad is observed ahead of the indenter and no elastic recovery occurs behind. Conversely, during scratching of a perfectly elastic material, an elastic deflection is observed ahead of the indenter and an equivalent recovery behind. As a consequence, in the elastic–plastic case, the combination of the elastic deflection and the identified plastic push pad in front of the indenter [27] leads to a geometric singularity represented by the inflexion point in the film (see Fig. 8) and causes detachment of the film/substrate interface.

Figure 9 describes, using simple geometric considerations, the chronology of the delamination process identified thanks to interferometric experiments:

1. Let D be a point within the periphery of the elastic deflection. When the tip moves, the deflection also moves and the velocity V_D of the point D is equal to that of the tip V_{tip}.
2. The inflexion singularity in the coating triggers cracking of the thin film/substrate interface. If P is a point at the tip of the interfacial crack, this point propagates with a velocity V_P which is greater than V_D.
3. When the front length l_f is equal to the elastic deflection length, the point P is equivalent to the point D, so that $V_P = V_D = V_{\text{tip}}$ and the crack propagates stably.

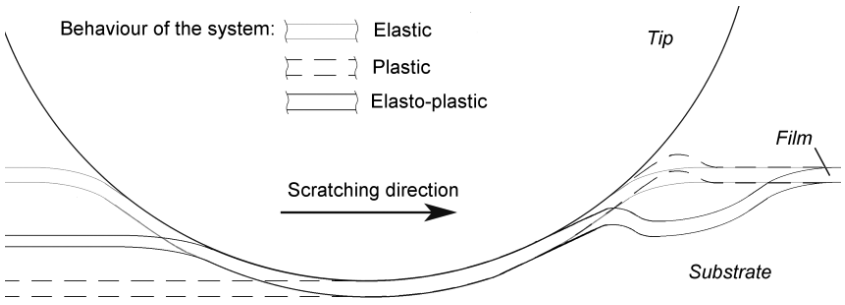

Fig. 8. Mechanism of the initiation of delamination – perfectly elastic, perfectly plastic and elastic-plastic behaviors of the system during scratching.

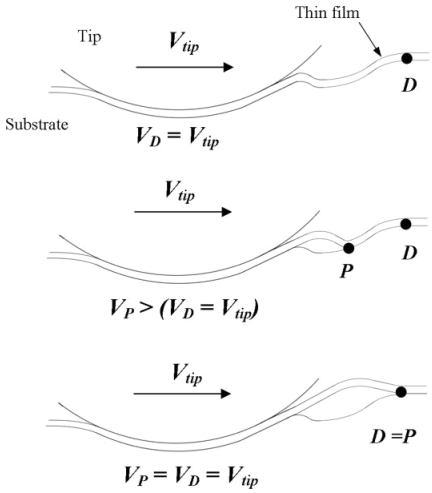

Fig. 9. Chronology of the occurrence of delamination — geometric and crack velocity considerations.

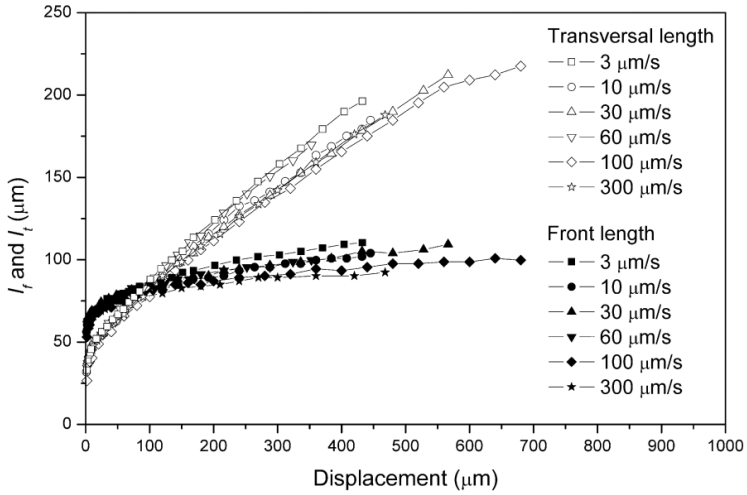

Fig. 10. Evolution of the front and transversal lengths (l_f and l_t) of the blister as a function of the tip displacement for different scratching speeds.

Subsequently, as seen in Fig. 7(b), the interfacial crack does not propagate further ahead of the indenter than the deflected area. Figure 10 shows accordingly that the front length l_f tends to a maximum value while the transversal length l_t continues to increase linearly as the blister propagates. Moreover, each side of the crescent blister can be assimilated to a straight-sided blister as described by Hutchinson *et al.* [3]. The main difference with respect to a straight-sided blister is that the sides of the

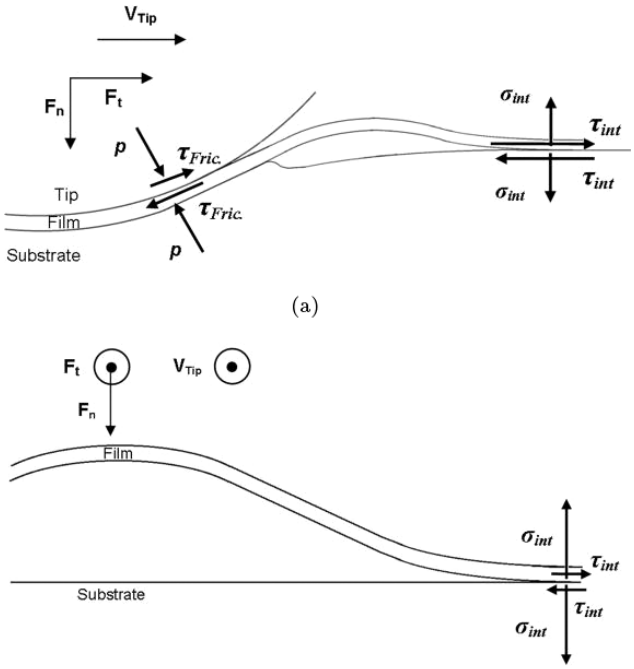

Fig. 11. Schematic representation of the cross-sections defined in Fig. 7 with the corresponding stress considerations: (a) cross-section A–A; (b) cross-section B–B.

crescent blister delaminate in front while the film plates back on the substrate at the rear. Nevertheless, the cross-sections of the crescents conserve the same size in accordance with the previously reported evolution of l_f, while the extremities of the crescent blister continue to propagate regularly as observed in straight-sided blisters.

It is also possible to obtain insight into the mechanisms of blister propagation by considering the stress modes at the tip of the interfacial crack in the different directions of blistering. Figure 11 schematizes the cross-sections A–A (a) and B–B (b) as defined in Fig. 7(b) during the blister propagation.

On the cross-section A–A, the crack has the size l_f induced by the elastic deflection of the substrate and is oriented in the scratching direction. Hence, the shear component of the stress τ_{int} is high due to the friction force acting in this direction. The stress mode II may be considered to predominate and thus the interfacial toughness is high as reported by Thouless *et al.* [2]. However, one may note that mode I resulting from the flexure of the film largely contributes as well to the frontal crack propagation, leading to a mixed I/II mode. However, the contribution of mode I at a larger scale

is not possible since the flexure of the film is finite due to the restricted zone submitted to the elastic deflection. On the cross-section B–B, the crack lies perpendicular to the scratching direction and the friction between the tip and the surface does not greatly influence the shearing in the interface. At the crack tip, the normal stress component σ_{int} predominates over the shear component τ_{int} and consequently mode I dominates the stress system, keeping the interfacial toughness low. Therefore, the crack propagates further if the tip continues to move, increasing the size l_t of the blister regularly as shown in Fig. 10. Considering blister geometry in the vicinity of the B–B cross-section, mode III may occur as well. The directional mechanism of blister propagation may be summarized by considering the ratios of the shear to the normal stress components:

$$\left(\frac{\tau_{\text{int}}}{\sigma_{\text{int}}}\right)_{A-A} > \left(\frac{\tau_{int}}{\sigma_{\text{int}}}\right)_{B-B}. \tag{2}$$

As the film is non-porous, it would also appear reasonable that the coating is plated back (and even stuck back as it will be discussed in Subsection 4.3) onto the substrate (although with poor adhesion as it will be discussed in Section 4) due to the atmospheric pressure. As seen in Fig. 12, the

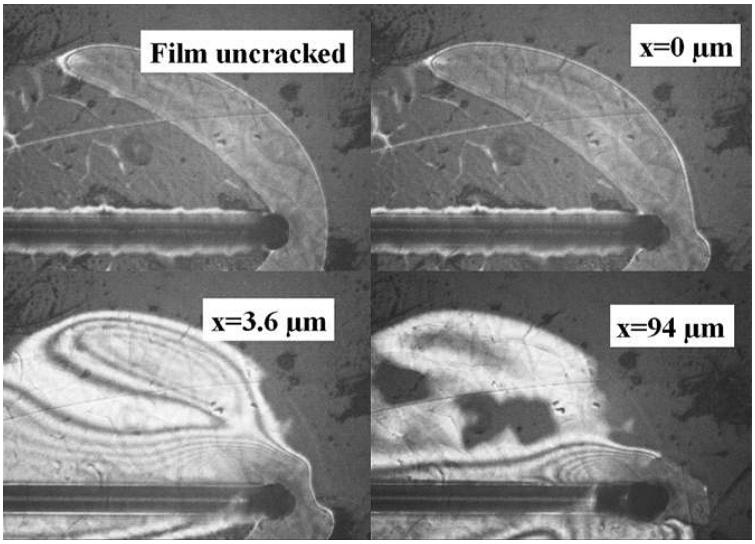

Fig. 12. While the film remains intact, the coating "sticks" back onto the substrate after passage of the blister and tip, due to the atmospheric pressure. After cracking of the film ($x = 0\,\mu$m), the atmosphere can penetrate the interface and on account of the lateral ploughing pad of the groove left on the substrate, delamination appears again. At $x = 3.6\,\mu$m, the tip plates the coating back onto the substrate, while for $x = 94\,\mu$m the tip only scratches the substrate and the coating located above the track left on the surface can rise further.

cracking within the film makes the atmosphere penetrate the interface and consequently the film delaminates.

Hence, on the observation scale of such experiments, the blister and total delaminated areas seem to grow continuously on the surface of the sample as long as the blistering system receives a steady supply of mechanical work, i.e. the tangential load F_t and scratching speed remain constant. The experiments performed for the present work support this view, since some crescent blisters that did not break by cracking before the scratching process had been stopped and the indenter lifted off the surface. After a few millimeters of scratching, these blisters were most of the time too large to be visualized on a single screen. However, some energetic considerations go against this assumption. Indeed, while growing, the blister needs more energy. In the present case, because the tangential force and friction are constant, the provided energy is also kept constant for a given time/displacement slot. This means the blister must stabilize in terms of shape and size by reaching a certain scratching distance under constant experimental conditions.

Figure 13 shows the end of the blistering sequence, as presented in Fig. 4, when it was possible to capture the full movie with no picture size restriction. When the blister has reached a certain size, it propagates with the indenter without increasing further in size (see Figure (9)).

As a consequence, one can define three regimes for the blistering process: (i) after its initiation, (ii) the blister proceeds first through a transient state during which it grows with respect to the scratching distance, and thus (iii) reaches in a second time a steady-state corresponding to the stable propagation of the blister.

The analysis of the latter images permits to extend the evolution of the delamination to the steady state of the blister propagation. The results are

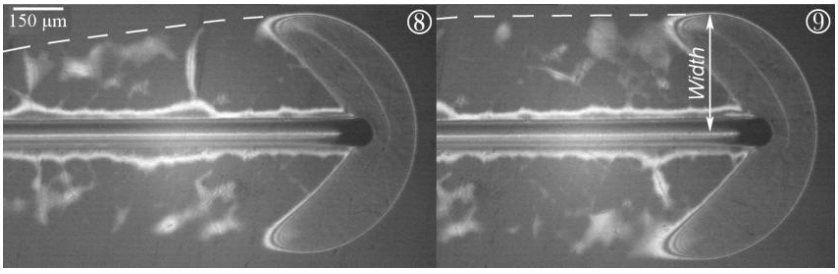

Fig. 13. End of the chronological sequence of the crescent blister growth reported as in Fig. 4. The dashed lines indicate the part of the thin film which has stuck back onto the substrate and shows clearly the constant propagation of the blister in Figure (9) which indicates the existence of a steady state propagation.

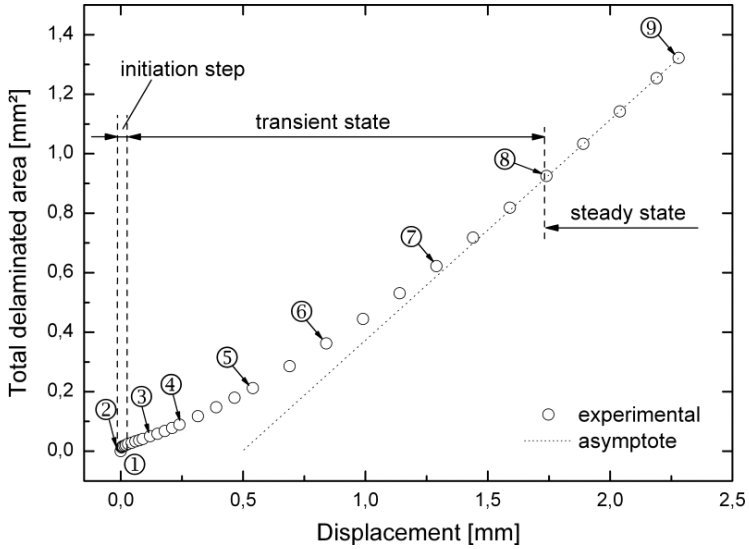

Fig. 14. Total delaminated area as a function of the scratching distance. The initiation step, the transient and steady states are defined and indexes (1)–(9) relating to Fig. 4 and 13 are indicated for convenience.

reported in Fig. 14. The total delaminated area corresponding to the steady state follows a linear evolution, as shown by the asymptote in Fig. 14. This confirms that in order to propagate the constant shaped and sized blister along the scratch, the provided energy has to be constant as well.

3.4. *General criteria for blistering and cracking phenomena*

It is clear that two criteria compete in the cracking and blistering behavior of the system: at low temperature, the cracking criterion is fulfilled before the blistering criterion, whereas at higher temperature (typically $> 20°C$) the blistering criterion is fulfilled first. The cracking criterion is directly governed by the high strain generated by the frontal push pad which occurs in the vicinity of the indenter in the coating, depending on its mechanical properties. Combination of the plastic push pad due to the imposed strain and the elastic deflection due to the loading indenter, gives a surface profile with the inflexion point ahead of the frontal push pad preceding the moving tip as reported in Fig. 8. The occurrence of blistering seems to be governed by this inflexion singularity as discussed previously and depends on the interfacial adhesion between the substrate and the film. Hence, both criteria are governed by the resulting scratching strain field undergone by the

material assembly: the temperature, scratching speed and Young's modulus of the substrate are the first-order parameters of the mechanism.

Actually, the scratching speed and temperature play an essential role in the Young's modulus of the substrate whereas the modulus of the coating remains *a priori* constant in the temperature range. As a consequence, these two parameters have inverse effects on the system response. In Fig. 15, the oriented abscissa axis represents increasing scratching speed, decreasing temperature and increasing Young's modulus of the substrate. The ordinate axis corresponds to a representative strain of the system as given by Johnson [28]:

$$\bar{\varepsilon} = \frac{E}{\sigma_y}\frac{a}{R}, \tag{3}$$

where E is Young's modulus, σ_y the yield stress, a the contact radius and R the radius of the tip.

It is thus possible to use Fig. 15 to compare the responses of similar systems (having the same interfacial strength and film thickness) to the scratching solicitation of a spherical indenter. In fact, an increase in $\bar{\varepsilon}$ results in an increase in the plastic component of the system deformation and leads to the formation of a larger plastic push pad ahead of and around

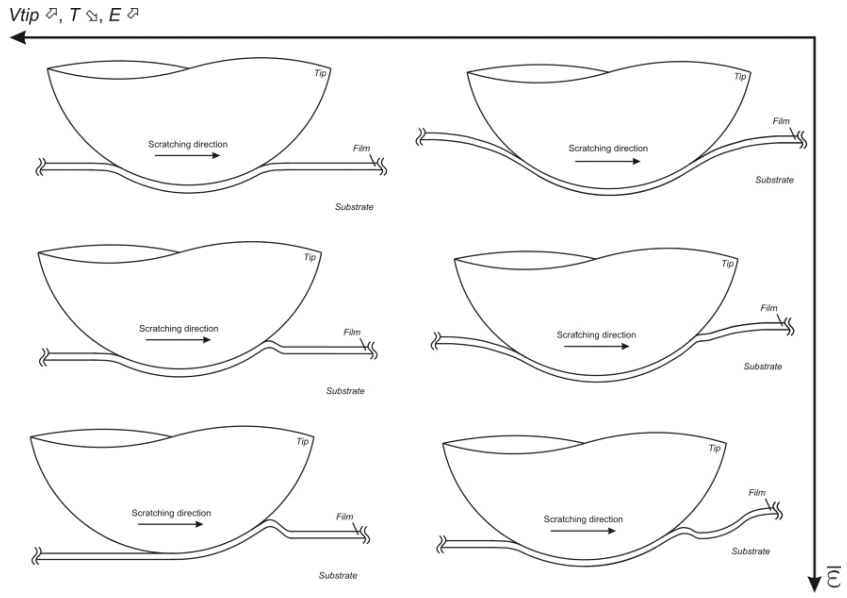

Fig. 15. Comparison of the responses of similar systems to the scratching solicitation of a spherical indenter, as a function of the test temperature, scratching speed, Young's modulus of the substrate and representative strain.

the indenter. As evoked above, this geometric singularity plays a crucial role in cracking of the film. This evolution is represented on the schemes of Fig. 15 on the ordinate axis. An increase in the Young's modulus of the substrate leads to a smaller elastic deflection of the system as is also shown in Equation (1). Combination of both phenomena described on this graph, i.e. plastic push pad and elastic deflection, gives a material profile with a second geometric singularity, named the inflexion point exhibited by the system ahead of the frontal push pad preceding the moving tip. This inflexion singularity determines the occurrence of blistering. The blistering criterion is therefore defined by a combination of both axes since it depends on the plastic flow and the elastic deflection, whereas the cracking criterion mainly depends on the plastic flow of the substrate which governs the maximum strain in the coating. To summarize, the blistering criterion may be followed on Fig. 15 along the diagonal, while the cracking criterion may be considered to follow the ordinate axis. The current experimental results can moreover be interpreted in the light of the previous considerations. High temperature has been reported to strongly favor blistering, whereas low temperature favors cracking. Thus, with increasing temperature (see Fig. 3), (i) cracking without blistering occurs, (ii) blistering occurs and propagates, soon followed by cracking which delineate the delaminated circular-shape zone and (iii) blistering occurs and propagates as a crescent blister until it collapses through cracking. This evolution is fully consistent with previous conclusions: as the Young's modulus of the substrate is divided by about 2 within the temperature range, the elastic deflection increases as well as the severity of the inflexion point reported in Fig. 15. The blistering mechanism becomes predominant over the cracking mechanism as the temperature rises.

These considerations lead to the following general conclusions. The present behavior may be regarded as typical for all coated systems with elastic coating and time and temperature dependency of the Young's modulus of the substrate (i.e. for most of polymeric substrates). Therefore, for the majority of non-brittle coatings on a poorly rigid substrate, the present results may partially explain why it is difficult to extrapolate the contact damage by changing the value of one property since damage criteria are intimately dependent.

4. Global Energy Balance of a Scratch

In this section, a global energy balance of the scratch has been developed, applied to the B-type sample, and discussed.

4.1. *Experimental case to be analyzed*

Since the material assembly consisting of the B-type sample is fully transparent, *in-situ* observation has been carried out for all scratching tests. As a function of the test conditions (indenter size and roughness, applied force) it was possible to achieve the propagation of a stabilized blister similar to the previously described process (see Section 3). It propagates at the same speed as the movement of the indenter over several hundreds of micrometers. However, as reported in the micrograph of a representative blister depicted in Fig. 16, it does not show a crescent-like shape. This exemplary test was conducted with a 250 μm radius spherical smooth indenter ($R_a = 0.005\,\mu$m) and with both constant scratching speed (10 μm/s) and normal load (0.25 N). Chronologically, the interfacial crack initiates and the resulting blister becomes progressively larger as it propagates. Thus, the blister reaches a certain size, and propagates at the same speed as the indenter without growing further: it constitutes the steady-state blister propagation. It ends when the test finishes or when cohesive cracking suddenly occurs within the film. The steady-state situation is favorable for an energetic analysis of the whole scratching process as reported in Ref. [18, 19]: contrary to the transient regime, the proportion of dissipations will remain constant and some simplifications will arise. Moreover, as reported by Dupeux [29], the initiation of interfacial cracking requires an energy which would appear to be hardly reproducible so that it is convenient to exclude the early phase of damage as well.

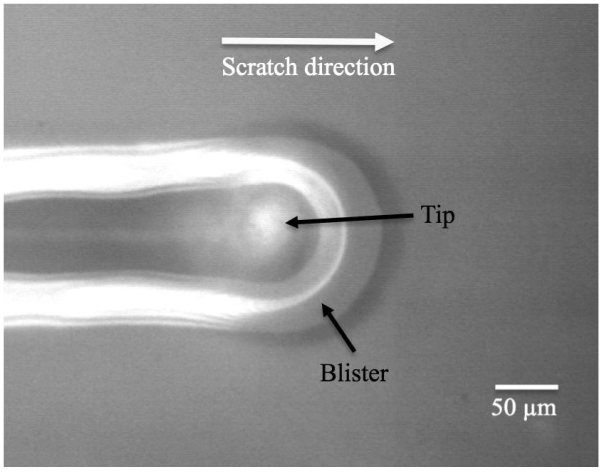

Fig. 16. *In-situ* micrograph of the resulting blister as the indenter scratches the material. In front of the indenter, the blister rises largely and hence the white light interferometric fringes are very close to each other.

4.2. *Description of the global energy balance*

The following energy balance model will be applied to the suitable damage previously described: the blister occurrence during its steady-state propagation, excluded the final cracking within the film for the sake of simplicity [18]. The variational form of the energy balance, i.e. considered between two distinct arbitrary time points during the steady-state propagation of the blister, can be written as follows:

$$\Delta W = \Delta E_F + \Delta E_D + \Delta E_E. \tag{4}$$

ΔW is the work provided by the loading indenter, while ΔE_F is the fracture energy which corresponds to fracture at the film/substrate interface in the delamination phenomenon, ΔE_E is the elastic energy due to reversible contributions and ΔE_D is the energy released in other dissipative phenomena not taken into account in the other terms. About the elastic energy, the loading indenter inputs elastic strain energy into the material system. Owing to the sliding process, this energy is constant during the test since the normal force remains constant, so $\Delta E_E = 0$ in Equation (4). Let d be the scratching distance covered by the indenter in the lapse of time considered in the variational energy balance. The expression describing the work corresponding to the indenter loading is clearly

$$\Delta W = F_t \cdot d, \tag{5}$$

with ~~F_n and~~ F_t the ~~normal and~~ tangential loads ~~respectively~~. μ_{app}, the apparent friction coefficient, is given by $\mu_{\text{app}} = F_t/F_n$. In the present case, the interfacial fracture energy ΔE_F corresponds to the energy dissipated by the propagation of the blister arising from fracture at the interface between the substrate and the coating. Since only the steady-state propagation of the blister is taken into consideration, ΔE_F is given by:

$$\Delta E_F = \Delta A_{\text{interf}} \cdot \Gamma_{\text{interf}}, \tag{6}$$

where $\Delta A_{\text{interf.}}$ is the area created at the interface and $\Gamma_{\text{interf.}}$ is the energy required to create one unit of interfacial new surface. The energy dissipation ΔE_D may be reduced in a first approximation to two terms: the first corresponding to the contribution of the true local friction and the second term corresponding to the plastic deformation of the system.

Formally, it gives

$$\Delta E_D = \Delta E_{D-\text{Friction}} + \Delta E_{D-\text{Plast}}. \tag{7}$$

The first term arises from the true local friction at the indenter/coating interface:

$$\Delta E_{D-\text{Friction}} = F_n \cdot \mu_{\text{local}} \cdot d, \tag{8}$$

with μ_{local} the local friction coefficient which can be deduced from experimental measurements using the method described by Lafaye *et al.* [24].

One should note that only the thin film could show plastic deformation or damage since critical loads related to the glass-made substrate were never reached. Actually, the coating deposited on the glass substrate is known to exhibit plasticity compared to the large elastic domain of the glass substrate. As a consequence, the plastic energy dissipated in the system will be exclusively restricted to the coating. Since measuring the dissipated energy by plasticity is not directly possible, its determination is the sensible point of this model. Indeed, whereas the previous studies [18, 19] neglect the plastic energy and then leads to the estimation of an upper bound of the film/substrate adhesion (and for this reason not given in the previous part), we propose here to write this energy as a function of two parameters that govern the contact behavior:

(i) the imposed deformation related to the a/R ratio (with a the contact radius and R the indenter radius);
(ii) the roughness R_a involved in the contact (i.e. the roughness of the indenter) related to the local plasticity induced by lower scale topography.

Then, it gives:

$$\Delta E_{D-\text{Plast}} = f\left(\varepsilon\left(\frac{a}{R}\right), R_a\right), \tag{9}$$

where f is a function depending on the variables in brackets.

Equation (4) may directly lead to the determination of the plastic energy if a test without blistering/cracking is achieved. The corresponding expression developed from Equations (4) and (7) is given by:

$$\Delta E_{D-\text{Plast}} = F_n \cdot d \cdot (\mu_{\text{app}} - \mu_{\text{local}}). \tag{10}$$

Experimental data show that it is even possible to fit the plastic energy in function of the mean strain by an exponential curve such as reported in Fig. 17 which corresponds to the test presented in Fig. 16.

Then, for one single test, the global energy balance derived from Equation (4) can be expressed as:

$$F_{t_{i,j}} \cdot d_{i,j} = \Delta E_{D-\text{Plast}_{i,j}} + F_{n_{i,j}} \cdot \mu_{\text{local}_{i,j}} \cdot d_{i,j} + \Delta A_{\text{interf}_{i,j}} \cdot \Gamma_{\text{interf}}. \tag{11}$$

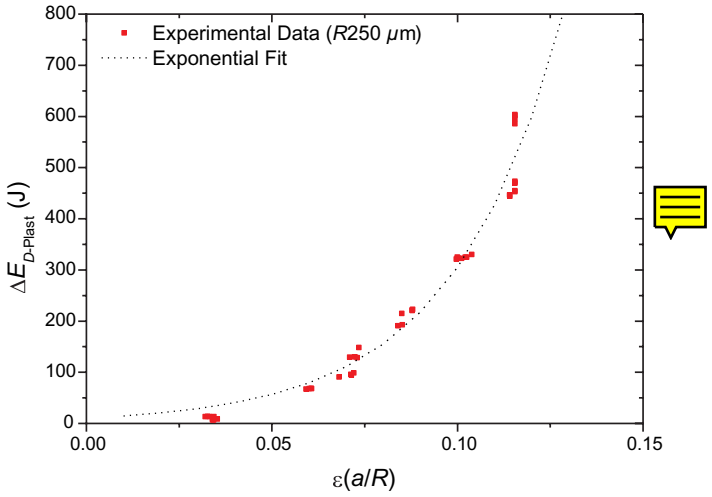

Fig. 17. Plastic energy generated by the mean deformation for one scratch test conducted with the 250 μm indenter, $R_a = 0.005\,\mu$m.

Table 1. Description of the equations associated to the tests for each indenter.

	Size-radius in μm		
in μm Roughness	**250**	**500**	**1,000**
0.005	Equation (1;1)	Equation (1;2)	Equation (1;3)
1.4	Equation (2;1)	Equation (2;2)	Equation (2;3)

The subscripts i and j are related to the radius and the roughness of the indenter respectively. Then, the previous equation can be named Equation (i,j). Table 1 summarizes the complete procedure drew by the experimental set of tests.

For each equation in Table 1, the input parameters are the geometry of blister (size of the delaminated area) and the characteristics of the contact (contact radius, indenter radius and roughness, and scratch distance). The output parameters are the total energy and the energy dissipated in friction. The unknowns are the components of the plastic energy (depending on both indenter radius and roughness through the exponential expression used in Fig. 17) and the interfacial adhesion between the film and the substrate. Consequently, the multi-indenter approach gives enough equations so as the system reported in Table 1 could be solved, thanks to a nonlinear least square method implemented in Matlab. The algorithm used was the *trust region reflective optimization* with a convergence criterion of 10^{-20} (50,000 maximum iterations) and a fit function tolerance of 10^{-15}. The maximum

number of function evaluations allowed was 60,000. A robust method was carried out to minimize the effect of excessive dispersed data on the fit. Indeed, the experimental data evaluated in terms of delaminated area are largely dispersed as reported thanks to boxplots in Fig. 18 with regard to the indenter radius for all roughness and to indenter roughness for all radii. Finally, thanks to this numerical procedure, it was possible to assess the adhesion through the determination of the best fit to the data. Table 2 gathers the results with regard to both roughness and size of the indenters.

The resulting values of interfacial adhesion are 65.8 and 78.8 J/m^2 for the single roughness considerations. The values are included between 85.8 and 103.2 J/m^2 for the single size considerations. The global fit for the multi-indenter approach, whatever the roughness and the size of indenter are, gives a value of 60.8 J/m^2 for the interfacial adhesion between the coating and the

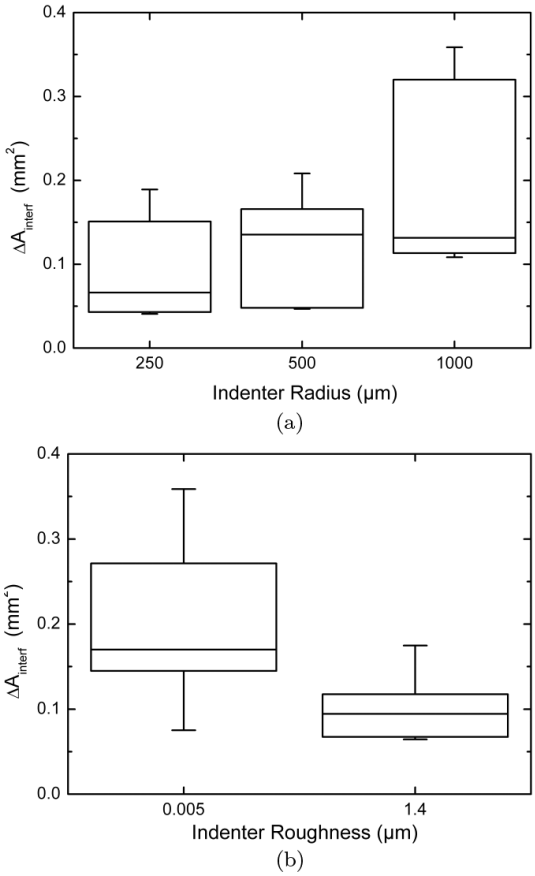

Fig. 18. Boxplot diagrams associated with the delaminated area as a function of (a) indenter radius and (b) indenter roughness.

Table 2. Interfacial adhesion values resulting from the least square method.

	Intender roughness (μm)	$\mathbf{\Gamma_{interf}}$ **(J/m^2)**	$\mathbf{R^2}$
Multisize	0.005	65.8	0.986
	1.4	78.8	0.987
	Indenter radius (μm)		
Multiroughness	250	103.2	0.990
	500	85.8	0.978
	1,000	97.6	0.978
Multisize and Multiroughness		60.8	0.979

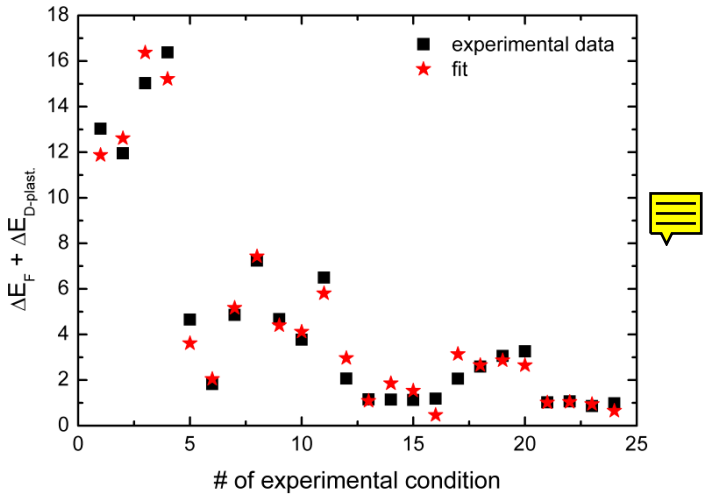

Fig. 19. Residuals related to multisize and multiroughness fit as a function of the number corresponding to each experimental condition.

substrate. One may note that the coefficient of determination R^2 is higher than 0.97 in every case. Moreover, the residuals of the fitted terms (i.e. $\Delta E_F + \Delta E_{D-\text{Plast}}$) are presented in Fig. 19 with regard to the experimental conditions. It confirms the reliability of the global fit.

4.3. *Contributions of Phenomena and Discussion on the Blistering Process*

As a result from the least square method applied to the system of equations, one can determine the different contributions of phenomena during scratching for each single experiment. As an example, Table 3 shows the balance involving the interfacial fracture, plasticity and friction in the case reported in Fig. 16 which consists of a stable blister propagation obtained during

Table 3. Contributions of phenomena in the concrete case of the scratch are reported in Fig. 16. Phenomena contributions during the steady-state propagation of the blister in terms of energies and corresponding tangential force.

Steady state $\approx$ **579** μ**m)**	**Loading indenter** $(F_t)\Delta W$	**Interfacial fracture** ΔE_F	**Dissipation —** ΔE_D	
			Plastic	**Friction**
Energy in μJ	23.8	5.0	9.1	9.7
Tangential force in mN	41.0	8.6	15.7	16.7

scratching with a 250 μm radius spherical indenter (R_a = 0.005 μm) and with both constant scratching speed (10 μm/s) and normal load (0.25 N). The steady-state propagation lasted about 579 μm and was fully considered in the data of Table 3. The input energy corresponds to 23.8 μJ and was dissipated in blister propagation, plastic flow and friction dissipation for 5.0, 9.1 and 9.7 μJ, respectively. Another manner to interpret these results is to consider the tangential force as the force of obstacle to the advance of the indenter. An obstacle force of 41 mN was recorded in average during the scratch test and could be dissociated following the distribution: 8.6 mN comes from the fracture associated to the blister propagation; the plastic flow contributes 15.7 mN to the tangential force; 16.7 mN is due to friction.

Using a least square method asks for caution about the uniqueness of the solution. The result concerning the interfacial adhesion reported in Table 2 from the multisize and multiroughness fit is consistent with the results for each set of indenter of same roughness or same size. Indeed, all the values of adhesion are in the same order of magnitude. These points tend to prove the reliability of the procedure although the number of different indenters to gain accuracy remains to be studied.

Thanks to this new method which permits to investigate precisely the phenomena involved while scratching and to quantify their corresponding energy dissipations, we can further explore the blistering process. Fig. 20 shows two scratching images taken *in-situ* that were superimposed. The sample is of A-type. The first picture corresponds to a first scratch, whereas the second picture relates to a second scratch conducted exactly at the same place and in the same experimental conditions as for the first try. Then the resulting second blister is initiated and can propagate freely on a previously delaminated area. Note that the picture of the second blister was taken at the end of its free propagation as its borders met the previously-delaminated boundary created by the first passing blister. However, up to this boundary (i.e. the chosen picture for the second blister), the second

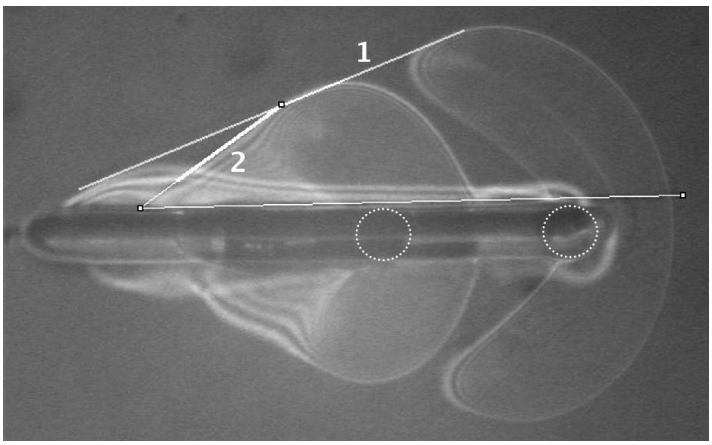

Fig. 20. Superimposition of two *in-situ* images corresponding respectively to a first scratch and a second one. This second try was conducted on the same place and in the same experimental conditions. Dashed circles represent the indenter place on the picture for both trials.

blister propagation does not appear to be influenced by any border effect. The slopes named 1 and 2 represent in first approximation the growth rate of the blister induced by the first and second tries, respectively. As it could be expected, the growth rate of the second try is far greater than during the first scratch. Thanks to the global energy balance, it was even possible to estimate that the adhesion corresponding to the second test (both tests were conducted up to the steady state) counts for about one-third of the initial adhesion obtained during the first scratch. This constitutes an estimation of the remaining interactions between the substrate and the coating when the latter has been stuck back as the first scratch passes by. One may note that the interactions remain pristine from pollution since no cracking within the coating occurs.

The global energy balance of the scratch can also be illustrated easily during an experimental test. Figure 21 depicts the contact sheet corresponding to a test sequence which consisted of two phases: (i) the growth of a large crescent blister (even larger than the screen size) under a constant normal load (first figure) and (ii) the blister evolution (following figures) after a partial normal load release that was performed between the first and second figures. Since the input energy is lower than during the first phase, the material cannot afford to spend enough energy to maintain the propagation of a blister of the same size. As a consequence, the blister irremediably decreases following a transient regime that leads to the blister disappearing. This shows that the energy balance makes sense and proves

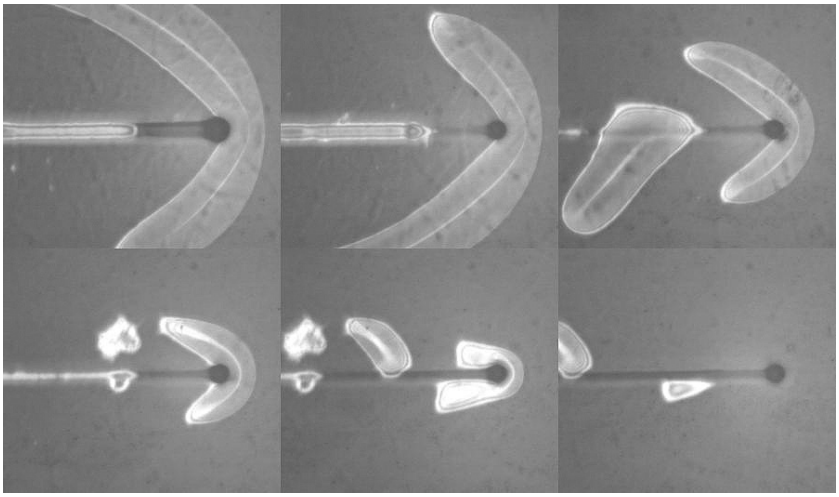

Fig. 21. Blister disappearing after a partial normal load release.

that it is definitely relevant to investigate the different phenomena involved during scratch tests.

5. Conclusions

The mechanical and tribological performances of polymeric surfaces can be improved by coating the material with an elastic thin film. However, contact damage limits the improvement of the response to scratching. An overview of the fracturing of such coatings deposited onto a viscoelastic — viscoplastic substrate (polycarbonate) has been drawn thanks to an experimental device which allows observation and recording of the true contact area during scratching.

Depending on the temperature and scratching speed, four types of fracture mechanisms were observed, combining delamination and blistering of the film and its cracking. At high temperature, a stable blister could propagate for several hundreds of micrometers. The description of the various damage mechanisms benefits greatly from the *in-situ* visualization since post-mortem observations are shown to be occasionally not relevant to distinguish them.

Quantitative results obtained by image analysis were discussed in terms of the temperature, scratching speed and damage mechanisms involved. Under all test conditions, the increase in the blister area followed a linear evolution domain where the blister area increased regularly.

The essential role in the delamination process of the elastic deflection of the substrate under the loading indenter was demonstrated using a

laser interferometric technique. The damage initiation and propagation mechanisms were discussed in the light of geometric, crack velocity and mixed-mode stress considerations. Qualitative criteria were proposed to discuss the occurrence of blistering and cracking phenomena.

A global energy balance of the scratch test has been developed and applied to the experimentally stable blistering propagation of a thin transparent UV-cured hybrid coating deposited onto an elastic substrate (glass). The main difficulty was to estimate the energy dissipated in plastic flow. Different tests were conducted with various probes: spheres with different radius and roughness. Thanks to this multicriteria approach, it was possible to fit a unique value of interfacial adhesion in the case of experimentally stable blistering propagations, consistent with the expected weak film bonding. It has also been established that the method permits to determine the dissipated plastic energy, leading to the full description of phenomena contributions during scratching.

The prospects of this work lie in taking into account the cohesive fracture that can occur in both substrate and coating as well as extending the energy balance to various other scratching cases.

References

1. Demirci, I., Gauthier, C. and Schirrer, R. (2005) Experimental study and mechanical analysis of damage of a thin polymeric coating during scratching: Relation between thickness and roughness, *Thin Solid Films*, 479, pp. 207–215.
2. Thouless, M. D., Hutchinson, J. W. and Liniger, E. G. (1992) Plane-strain, buckling-driven delamination of thin films: Model experiments and Mode-II fracture, *Acta Metall. Mater.*, 40, pp. 2639–2649.
3. Hutchinson, J. W. and Suo, Z. (1991) Mixed mode cracking in layered materials, *Adv. Appl. Mech.*, 29, pp. 64–191.
4. Moon, M. W., Jensen, H. M., Hutchinson, J. W., Oh, K. H. and Evans, A. G. (2002) The characterization of telephone cord buckling of compressed thin films on substrates, *J. Mech. Phys. Solids*, 50, pp. 2355–2377.
5. Faou, J. -Y., Parry, G., Grachev, S., Barthel, E. (2015) Telephone cord buckles — A relation between wavelength and adhesion, *J. Mech. Phys. Solids*, 75, pp. 93–103.
6. Kriese, M. D., Boismier, D. A., Moody, N. R. and Gerberich, W. W. (1998) Nanomechanical fracture-testing of thin films, *Eng. Fract. Mech.*, 61, pp. 1–20.
7. Bull, S. J. (1997) Failure mode maps on the thin film scratch adhesion test, *Tribol. Int.*, 30(7), pp. 491–498.
8. Bull, S. J. and Berasetegui, E. G. (2006) An overview of the potential of quantitative coating adhesion measurement by scratch testing, *Tribol. Int.*, 39(2), pp. 99–114.
9. Malzbender, J., den Toonder, J. M. J., Balkenende, A. R. and de With, G. (2002) Measuring mechanical properties of coatings: a methodology applied

to nano-particle-filled sol-gel coatings on glass, *Mater. Sci. Eng. Rep.*, 36, pp. 47–103.

10. Cook, R. F. and Pharr, G. M. (1990) Direct observation and analysis of indentation cracking in glasses and ceramics, *J. Am. Ceram. Soc.*, 73(4), pp. 787–817.
11. Le Houerou, V.,Sangleboeuf, J. C.,Deriano, S.,Rouxel, T. and Duisit, G. (2003) Surface damage of soda-lime-silica glasses: Indentation scratch behavior, *J. Non-Cryst. Solids*, 316(1), pp. 54–63.
12. Venkataraman, S.,Kohlstedt, D. L. and Gerberich, W. W. (1992) Microscratch analysis of the work of adhesion for Pt thin films on NiO, *J. Mater. Res.*, 7(5), pp. 1126–1132.
13. Gauthier, C.,Lafaye, S. and Schirrer, R. (2001) Elastic recovery of a scratch in a polymeric surface: Experiments and analysis, *Tribol. Int.*, 34(7), pp. 469–479.
14. Mittal, K. L. (1978) *Adhesion Measurement: Recent Progress, Unsolved Problems, and Prospects.* ASTM Special Technical Publication, (640), pp. 5–17.
15. Thouless, M. D. (1998) An analysis of spalling in the microscratch test, *Eng. Fract. Mech.*, 61, pp. 75–81.
16. Volinsky, A. A., Moody, N. R. and Gerberich, W. W. (2002) Interfacial toughness measurements for thin films on substrates, *Acta Mater.*, 50, pp. 441–466.
17. Ritter, J. E.,Lardner, T. J.,Rosenfeld, L. and Lin M. R. (1989) Measurement of adhesion of thin polymer coatings by indentation, *J. Appl. Phys.*, 66(8), pp. 3626–3634.
18. Le Houérou, V.,Gauthier, C. and Schirrer, R. (2008) Energy based model to assess interfacial adhesion using a scratch test, *J. Mater. Sci.*, 43(17), pp. 5747–5754.
19. Le Houérou, V.,Gauthier, C. and Schirrer, R. (2010) Mechanical analysis of the blistering of a thin film deposited on a glassy polymer, *Tribol. Int.*, 43(1–2), pp. 129–135.
20. Belon, C.,Chemtob, A.,Croutxé-Barghorn, C.,Rigolet, S.,Le Houérou, V. and Gauthier, C. (2010) Combination of radical and cationic photo processes for the single-step synthesis of organic–inorganic hybrid films, *J. Polym. Sci. Part A: Polym. Chem.*, 48(19), pp. 4150–4158.
21. Gauthier, C. and Schirrer, R. (2000) Time and temperature dependence of the scratch properties of poly(methylmethacrylate) surfaces, *J. Mater. Sci.*, 35(9), pp. 2121–2130.
22. Gauthier, C.,Durier, A.-L.,Fond, C. and Schirrer, R. (2005) Scratching of a coated polymer and mechanical analysis of a scratch resistance solution, *Tribol. Int.*, 39, pp. 88–98.
23. Le Houérou, V.,Robert, C.,Gauthier, C. and Schirrer, R. (2008) Mechanisms of blistering and chipping of a scracth-resistant coating, *Wear*, 265(3–4), pp. 507–515.
24. Lafaye, S.,Gauthier, C. and Schirrer, R. (2005) A surface flow line model of a scratching tip: Apparent and true local friction coefficients, *Tribol. Int.*, 38, pp. 113–27.
25. Loubet, J. L.,Georges, J. M. and Meille, G. (1986) *Vickers Indentation Curves of Elastoplastic Materials, in Microindentation Techniques in Materials*

Science and Engineering, ASTM STP 889 (Blau, P. J. and Lawn, B. R. American Society for Testing and Materials, Philadelphia), pp. 72–89.
26. Sneddon, I. N. (1965) The relation between load and penetration in the axisymmetric Boussinesq problem for a punch of arbitrary profile, *Int. J. Eng. Sci.*, 3, pp. 47–57.
27. Bucaille, J. L.,Gauthier, C.,Felder, E. and Schirrer, R. (2006) The influence of strain hardening of polymers on the piling-up phenomenon in scratch tests: Experiments and numerical modelling, *Wear*, 260(7–8), pp. 803–814.
28. Johnson, K. L. (1985) *Contact Mechanics* (Cambridge University Press, Cambridge).
29. Dupeux, M. (2004) Measurement of interfacial crack propagation energy-related problems and examples of results of buldge-and-blister test, *Mécanique Industries*, 5(4), pp 441–450.